Energy Conversion and Management 352 (2026) 121093

Contents lists available at ScienceDirect

Energy Conversion and Management

journal homepage: www.elsevier.com/locate/enconman

A comparative conceptual analysis of CO_2 heat pump dryers with closed-loop and open-loop air cycles

Jay Wang [1]

School of Engineering, Computer & Mathematical Sciences, Auckland University of Technology (AUT), Auckland 1010, New Zealand

ARTICLE INFO

Keywords:
CO_2 heat pump dryer
Open-loop air cycle
Closed-loop air cycle
Specific moisture extraction rate
Drying time

ABSTRACT

This study has comprehensively compared and analysed CO_2 heat pump dryers operating under closed-loop and open-loop air cycles to evaluate their energy efficiency and drying performance. Unlike the conventional closed-loop air cycle that uses dry recirculated air as its inlet, the open-loop air cycle operates only with fresh ambient air. The physical models and working principles have been illustrated using psychrometric charts, and the influence of moisture variation has been considered in the fin-and-tube heat exchanger design for both the gas cooler and the evaporator. In the case study under typical hot and humid climate conditions (ambient temperature of 40 °C), the simulation compares three cycles over an air mass flow rate ranging from 0.5 kg/s to 1 kg/s. The open-loop air cycle with a wet air outlet achieves the largest heating capacity, i.e.: 17.44 kW at 1 kg/s, because the air is cooled in the evaporator first, allowing a greater temperature rise in the gas cooler. The open-loop air cycle with a dry air outlet produces the highest air temperature after the gas cooler, i.e.: 60.8 °C at 0.5 kg/s, which increases the air's moisture absorption capacity. Compared with the closed-loop air cycle, the open-loop air cycle with dry air outlet proves more efficient for drying, delivering a shorter drying time (27.77 min at 0.5 kg/s) and a higher drying efficiency (0.8640 kg/kWh at 0.5 kg/s). Although the open-loop air cycle with a wet air outlet achieves the highest coefficient of performance of 2.31 at 1 kg/s, its drying performance declines obviously at higher mass flow rates, with specific moisture extraction rate dropping to 0.0767 kg/kWh. Overall, the configuration of open-loop air cycle with dry air outlet is the superior option, as it combines the shortest drying time and the highest specific moisture extraction rate, which are two critical metrics for heat pump dryers.

1. Introduction

The growing emphasis on sustainable energy use and environmentally friendly technologies has accelerated the adoption of heat pump-assisted drying system. Among the available working fluids on the market, CO_2 has attracted considerable attentions due to its green and safe characteristics [1], including its ozone depletion potential (ODP) of 0, global warming potential (GWP) of 1, non-flammability, and non-toxicity. CO_2 also demonstrates competent thermodynamical performance in transcritical cycles, which are advantageous for high-temperature drying processes [2]. Its high volumetric cooling capacity enables compact system designs, while its ability to achieve high discharge temperatures makes it particularly suitable for drying operations that require elevated air temperatures [3]. This allows CO_2 heat pumps not only to reduce energy use but also to maintain product quality in applications such as food preservation, pharmaceuticals, textiles, and agricultural products [4].

There are several advantages using heat pump technology for drying purposes, including its energy-saving potential and precise control of the operating parameters, such as drying temperature and air humidity [5]. Drying process is among the most energy-demanding unit operations, which can account for as much as 15 % of total industrial energy consumption [6]. Industrial drying processes often result in considerable energy wastage [7]. It was reported by Mujumdar et al. [8] that drying can account for as much as 70 % of total energy use in wood product manufacturing, 50 % in producing finished textile fabrics, and over 60 % in on-farm corn production. Consequently, effective energy management is crucial in drying operations and improving energy efficiency plays a major role in reducing overall operating costs [9]. Conventional dryers typically operate with low energy efficiency, with values around 35 % representing the upper performance range [10]. Strommen et al. [11] reported that heat pump dryers can consume at least 60 % and up to 80 % of less energy compared to conventional dryers under the same operating temperature, which can prove that the heat pump dryer is a feasible and promising option for the end-users who are seeking to

E-mail address: jay.wang@aut.ac.nz.
[1] Auckland University of Technology, ECMS (C-46), WZ Building, 6 St Paul Street, Auckland 1010, New Zealand.

https://doi.org/10.1016/j.enconman.2026.121093
Received 12 September 2025; Received in revised form 7 December 2025; Accepted 15 January 2026

Nomenclature

AH	absolute humidity, g/kg$_{dry\ air}$
Cp	specific heat capacity, kJ/kg·K
D	diameter, m
D_h	Hydraulic diameter, m
Fp	fin pitch, m
f	motor speed frequency, Hz
h	enthalpy, kJ/kg
h_o	air heat transfer coefficient, W/m^2·K
h_i	CO_2 heat transfer coefficient, W/m^2·K
j	colburn j-factor
k	thermal conductivity, W/m·K
Le	effective fin length, m
m	fin parameter
$\dot{m}$	mass flow rate, kg/s
Nu	nusselt number
P	pressure, bar
P_t	transverse tube pitch, m
P_l	longitudinal tube pitch, m
Pr	prandtl number
W	energy consumption, kJ or kWh
$\dot{Q}$	heat transfer rate, W or kW
r	compresssion ratio
Re	reynolds number
R_w	specific gas constant of water vapour, J/kg·K
RH	relative humidity, %
t	time, s
T	temperature, °C
ΔT	temperature difference, °C or K
u	dynamic viscosity, kg/m.s
$\dot{V}$	volumetric flow rate, m^3/s
$\dot{W}$	power input, kW
x	humidity ratio, g/kg $_{dry\ air}$

Greek symbols

η	efficiency
η_v	volumetric efficiency
ρ	density, kg /m^3

Abbreviation

COP	coefficient of performance
GWP	global warming potential
ODP	ozone depletion potential
RPM	revolution per minute
SMER	specific moisture extraction rate, kg/kWh
TES	thermal energy storage
UP	ultrasonic pretreatment

Subscripts

comp	compressor
con	condenser
cri	critical
dis	discharge
dew	dew point
eva	evaporation
isentr	isentropic
ref	reference
sat	saturated
suc	suction
sen	sensible
super	supercritical
tot	total
w	water

reduce the excessive energy consumption associated with directly heated dryers.

Heat pump dryers can be generally categorised into the closed-loop and open-loop configurations. The most common closed-loop heat pump dryer circulates dry air within the system. Moist air (after absorbing the moisture from the material) is dehumidified at the evaporator and reheated by the condenser before being recirculated. This type of system requires higher initial expenditure for ductwork installation, complex system control, and may result in longer drying time. Open-loop heat pump dryers replace the conventional electrical heater with a heat pump condenser, drawing ambient air rather than recirculated dry air, and ultimately discharging the moist or dry exhaust air into the surroundings or reusing it in other processes. This type of system is more straightforward with lower capital cost and shorter drying time, compared to those of the closed-loop systems.

Despite the growing interest in CO_2 heat pump technology, research on open-loop air cycle configurations remains limited, and comprehensive comparisons with closed-loop systems are still lacking. Most previous studies have still focused on closed-loop designs due to their relatively higher energy efficiency and established operational stability [12]. To address the low energy utilization observed in the middle and later stages of closed-cycle drying, Zhou et al. [12] conducted an experimental study on a closed-cycle heat pump dryer enhanced with ultrasonic pretreatment (UP) for lemon slices drying. It was revealed that the UP process increased the porosity of lemon slices by around 50 % at the power of 150 W and can decrease the drying time by up to 30.7 %. Xie et al. [13] developed a dynamic model for a closed-loop heat pump dishwasher dryer, accurately capturing transient air-side and refrigerant-side behaviour with errors below 20 %. Parametric results showed that reducing the expansion valve opening from 100 % to 20 % enhanced dehumidification by 21.3 % but reduced coefficient of performance (COP) by 11.9 %. Wu et al. [14] investigated a three-stage closed-loop heat pump drying system for deep sludge drying under the temperatures of 30 °C, 40 °C, and 50 °C, respectively. The optimal durations, including 2.4897 h (low-temperature), 2.4878 h (medium-temperature), and 1.5879 h (high-temperature), which enabled the closed-loop system to achieve an energy efficiency score of 0.8998, a drying effect of 0.8836, and a total drying time of 6.5654 h. Ni et al. [15] developed an improved closed-loop heat pump dryer by adding heat exchangers on both the air and refrigerant sides to enhance temperature matching and energy use. Thermodynamic and exergy analyses identified CO_2/R290 (20 %/80 %) as the optimal zeotropic working fluid. This mixture significantly outperformed R134a, increasing COP and specific moisture extraction rate (SMER) by up to 33.66 % and 41.50 %, respectively, while reducing refrigerant charge and lowering exergy destruction. The addition of CO_2 also narrowed the flammability range, which improves system safety.

Bharathi and Kalaiselvam [16] evaluated a closed-loop desiccant wheel-integrated heat pump dryer for low-temperature drying of pony fish. Increasing the temperature from 40 °C to 50 °C raised the drying rate to 8.18 % wb/h, cut drying time to 5.5 h, and increased moisture diffusivity to 1.87 × 10^{-9} m^2/s. The study shows that the closed-loop cycle delivers efficient drying with good product quality, especially at 45–50 °C. Jo et al. [17] investigated a closed-loop heat pump tumble dryer, to examine how fabric type and operating conditions affect heat and mass transfer. The experimental study revealed that: under maximum-SMER settings, SMER increased by 3.1–4.5 % compared with conventional operating modes. Hou et al. [18] studied a closed-loop transcritical R744/R290/R32 heat pump intermittent dryer for corn kernels and showed that intermittent operation improves performance.

Compared with continuous drying, intermittent ratios of 1/6–4/6 increased drying rate by 3.79–19.49 % and SMER by 29.67–52.21 %, while reducing crack rate by 8.70–26.09 %. Guan et al. [19] evaluated a closed-loop intermittent variable-temperature potato drying system using a heat pump integrated with a rock thermal energy storage (TES) bed. Extending the TES charging period improved charge and discharge efficiency by 22.9 % and 27.9 %, reduced exergy loss by 19.16 %, and raised overall thermal efficiency by 24.6 %. Hou et al. [20] developed a closed-loop solar-mixed-source heat pump dryer and assessed its seasonal performance. In summer, the solar-air-source mode cut energy use by 38.11 % and raised COP and SMER by 48.82 % and 38.36 %, respectively. Optimizing the start-stop temperature range (28–54 °C) increased COP to 4.03 (+5.5 %) and boosted the weekly average COP by 6.21 %. The validated model identified optimal operating ranges of 30–35 °C in spring and 12–21 °C in winter, establishing a full four-season control strategy for the closed-loop system. Aktekeli et al. [21] developed and tested a compact bi-fluid PVT-assisted heat pump dryer under low-temperature conditions. PVT integration boosted electrical efficiency by up to 18.2 % and achieved thermal efficiencies of 42–55 %.

However, closed-loop heat pump dryers are associated with the high capital costs [22], technical complexity [23], and limited suitability for applications that demand shorter drying cycles [24]. Moreover, although CO_2 heat pumps have been considered as a promising alternative to conventional electric dryers, there remains limited research directly comparing open-loop and closed-loop configurations under identical operating conditions. Existing studies have not distinguished between different types of open-loop cycles (either with dry air outlet or wet air outlet) nor examined how their thermodynamic behaviour differs from that of closed-loop systems. In the case of open-loop systems, the choice of ambient air inlet location and the variation in inlet air conditions can influence drying performance, while these mechanisms have not been systematically investigated and quantified. This absence of comparative and mechanistic analysis represents a knowledge gap and limits practical engineering guidance regarding when open-loop or closed-loop air cycles are more advantageous.

The aim of this study is to conduct a conceptual analysis and performance comparison of CO_2 heat pump dryers operating under open-loop and closed-loop air cycles, to evaluate their energy efficiency, drying performance, and practical feasibility under different operating conditions. To achieve the aim, the system configurations and physical models of CO_2 heat pump dryers are developed and analysed for both open-loop and closed-loop air cycles, with performance assessed based on key operating parameters, including energy consumption, COP, SMER, and drying time. In addition, the study investigates the influence of varying air inlet locations on open-loop systems and aims to identify the advantages, limitations, and trade-offs between closed-loop and open-loop air cycles. In an open-loop air cycle, only one part of the cycle requires matching the inlet conditions, whereas in a closed-loop air cycle, both the heating and cooling processes must be simultaneously controlled to satisfy the required parameters at both the inlet and outlet. Unlike existing research, this study provides the first unified modelling framework that compares three distinct air-cycle configurations, including closed-loop, open-loop with dry air outlet, and open-loop with wet air outlet, under identical operating parameters, enabling a mechanistic evaluation of their thermodynamic behaviours. This approach introduces new insights into how moisture absorption, air heating characteristics, and system constraints differ across the three cycles.

This study contributes to advancing CO_2 heat pump drying technology, which represents a promising direction for sustainable thermal processing in industries such as food, agriculture, and textiles. By clarifying the thermodynamic behaviour and performance differences between open-loop and closed-loop air cycles, the findings provide new engineering guidance and practical criteria for selecting cycle configurations, thereby supporting the future optimisation and wider industrial adoption of environmentally friendly drying technologies.

2. System configuration and cycles

The configuration of the CO_2 heat pump, along with detailed descriptions of the closed-loop and open-loop air cycles, is presented in this chapter. In addition, the fundamental working principles are illustrated and explained using psychrometric charts.

2.1. Heat pump

The configuration of the CO_2 heat pump system shown in Fig. 1 is used for analysis in this conceptual study. Both the gas cooler and evaporator operate within the air cycle, that is, the air temperature is

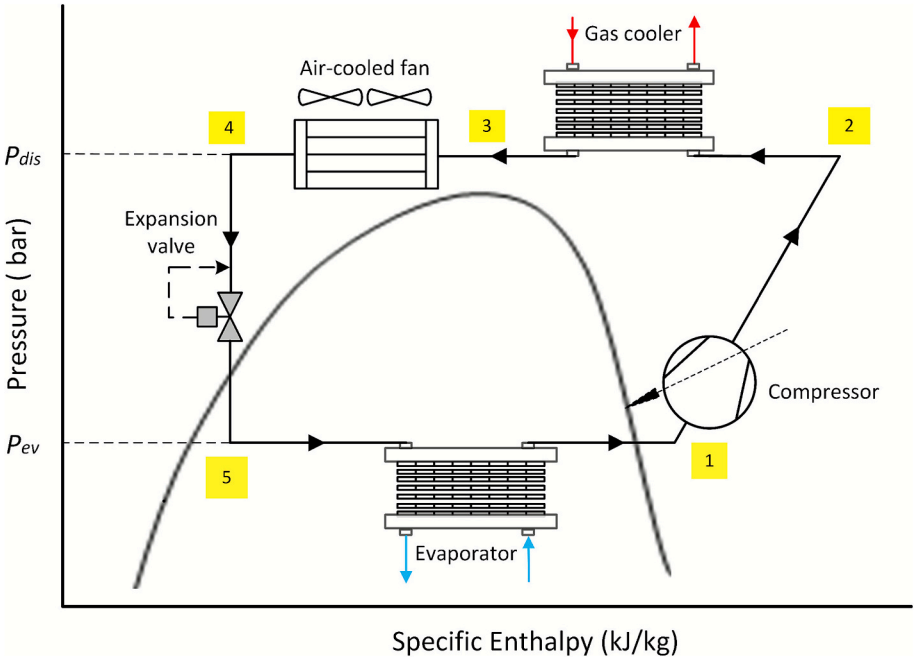

Fig. 1. Transcritical CO_2 heat pump system in the *P-h* cycle.

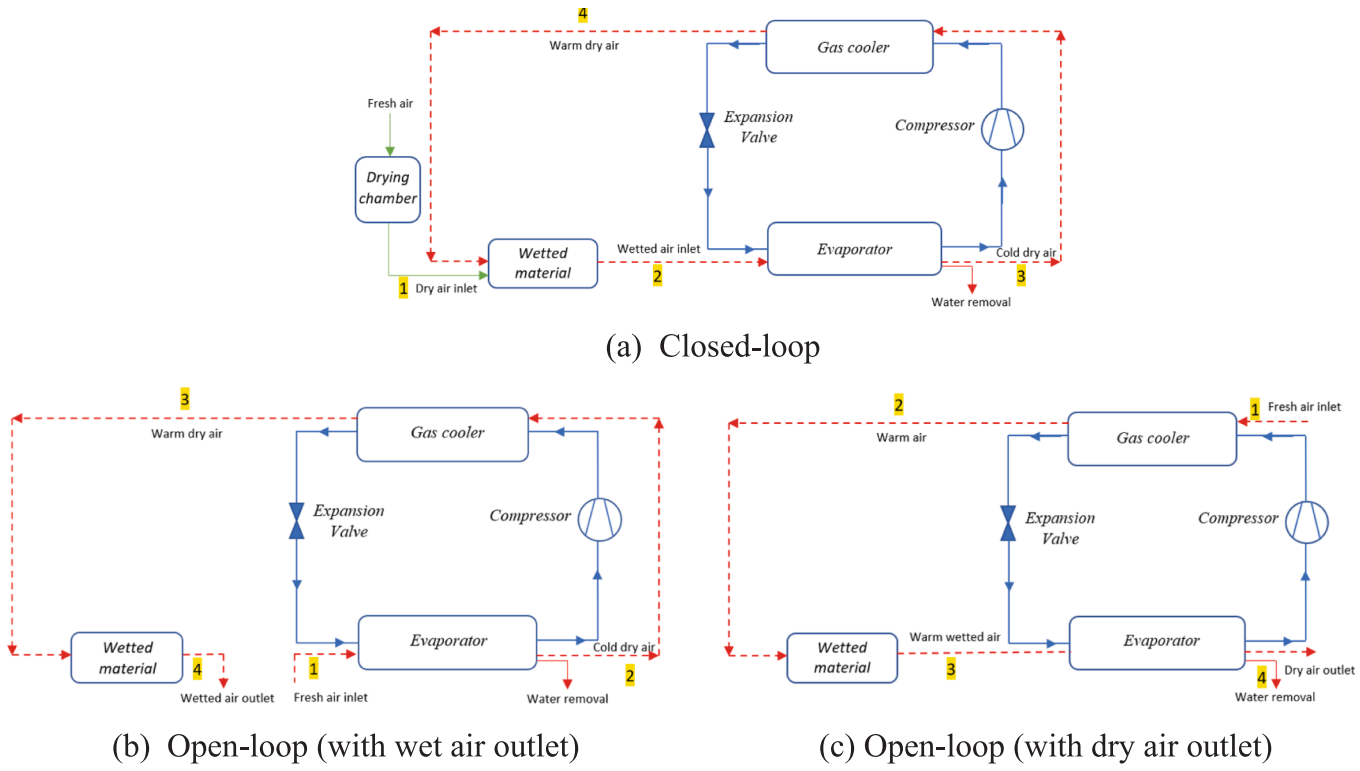

Fig. 2. The physical models of the CO_2 heat pump dryer.

heated by the CO_2 gas cooler while moisture is removed during the cooling process inside the evaporator. Since the study is based on theoretical analysis while considering practical aspects of real-world systems, the process from state 3 to state 4 includes a subcooling process, which helps the CO_2 heat pump system maintain stable operation when the gas-cooler inlet temperature or mass flow rate fluctuates. Additionally, if the gas cooler is temporarily inactive, the air-cooled fan can maintain airflow circulation to ensure the system continues operating under safe conditions. It is noted that a CO_2 heat pump system operates in a transcritical cycle with the operating pressure typically higher than 75 bar.

2.2. Closed and open-looped air cycles

The working cycles in the air-drying process can be illustrated using physical models, where Fig. 2(a) represents a closed-loop cycle with the dry air inlet, Fig. 2(b) shows an open-loop cycle with fresh air inlet (and wet air outlet), and Fig. 2(c) is an open-loop cycle with the fresh air inlet (and dry air outlet). In a closed-loop cycle, the process air is fully recirculated within the system rather than replaced with fresh ambient air. After leaving the drying chamber [25], it is the dry air at the inlet (state 1). The moisture contained in the material is then picked up by the dry air, leading to moist air at state 2. During the evaporation process from state 2 to 3, the wet air will be first cooled sensibly to its dew point, followed by simultaneous cooling and dehumidifying, during which water vapour gradually condenses from the air. From state 3 to 4, the cold dry air is heated through a fin-and-tube heat exchanger (the gas cooler), producing warm dry air at state 4, which is then followed by the moisture absorption process in another cycle. It should be clarified that the closed-loop air cycle does not continuously draw in ambient fresh air. Fresh air enters the drying chamber only during the initial system setup. After this initial entry, the same air is dried, conditioned, and fully recirculated within the loop.

In terms of the open-loop air cycles, the fresh air inlet can be positioned at either the evaporator entry or the condenser entry, with the outlet of the wet air or dry air, respectively. Since the air is not recirculated in an open-loop cycle, the state at the outlet does not need to match the state at the inlet of the loop. In other words, the entire heating or cooling capacity produced on the refrigerant side can be fully utilized for air heating or cooling independently, only depending on the effectiveness of the heat exchanger. The drying temperature can be then unconstrained, as it is only restricted by the maximum withstand temperature of the material and the discharge temperature post-compression. It should be noted that state 1 to 2, in Fig. 2(b), will not directly affect the material drying process, since only the moisture contained in the fresh air will be dehumidified, leading to the dry air being looped, while the process from state 1 to 2 in Fig. 2(c) can raise the temperature of the fresh air even further, enhancing its capacity to absorb moisture from the wet material.

2.3. Working principles in psychrometric cycles

The psychrometric diagrams of the air-drying process with the inlets of dry air and fresh air are described in Fig. 3, where the states pointed out in the diagrams are consistent with those in Fig. 2. All loops contain the air heating process, the moisture absorption process and the moisture removal process (dehumidifying process). As can be seen from the figures, the humidity ratio (x) remains constant when the dry air is being heated up. There is approximately an isenthalpic process during the moisture absorption process, as the moisture from the material increases the humidity ratio while the air temperature decreases due to the effect of the heat of evaporation. During the moisture removal process, the humidity ratio remains constant as long as only sensible cooling occurs before the air reaches its dew point, followed by the change of both the sensible and latent heat, i.e. both the air temperature and humidity ratio decrease at a relative humidity (RH) of 100 %.

In a closed-loop air cycle, as shown in Fig. 3(a), the amount of heat capacity used for air heating (from state 3 to 4) needs to be matched with the useful cooling capacity generated for dehumidifying from state 2 (or 2′) to 3, when the air volumetric flow rate remains constant. However, in

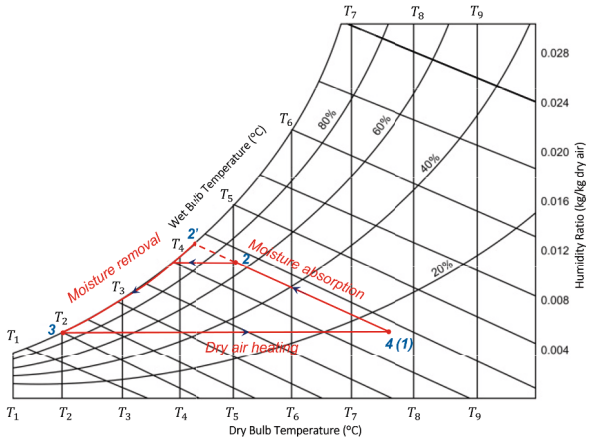

(a) Closed-loop

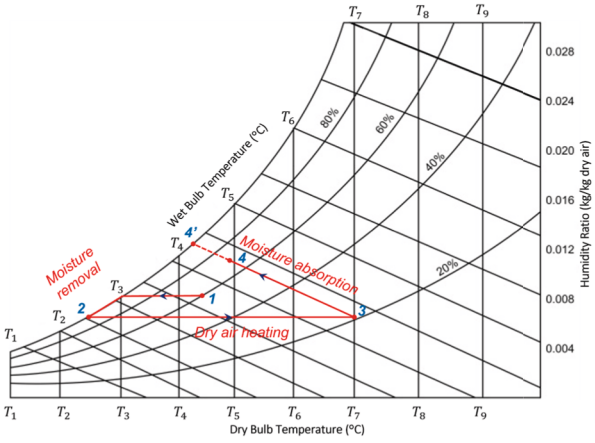

(b) Open-loop (with wet air outlet)

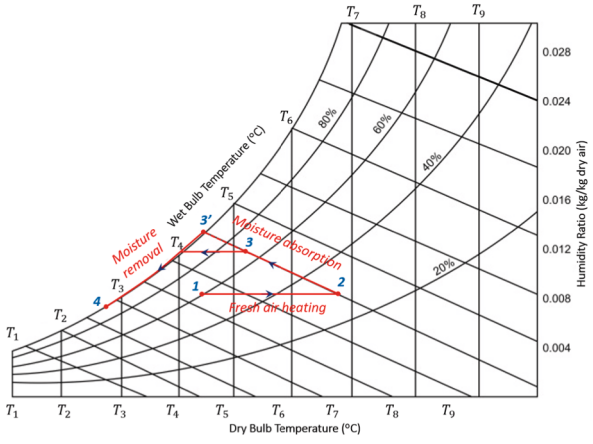

(c) Open-loop (with dry air outlet)

Fig. 3. Psychrometric charts of the air cycles.

an open-loop cycle with wet air outlet, as shown in Fig. 3(b), the useful heating capacity (from state 2 to 3) can be larger than the useful cooling capacity (from state 1 to 2), possibly leading to an even higher air temperature at state 3. Since the wet air after absorption does not need to be returned in an open-loop cycle, the outlet air state is not constrained by the inlet conditions. Therefore, the open-loop air cycle can deliver the air to any temperature without penalty, i.e. making more use of the rejected heat compared to that in the closed-loop air cycle. In view of the current system settings, the air volumetric flow rate is primarily designed based on the required cooling capacity. Practically, the air flow rate also depends on the electrical power input to the fan, the noise level, and the size of the evaporator [26]. In an open-loop cycle with dry air outlet, as shown in Fig. 3(c), the fresh air can be heated up to a relatively high temperature at state 2 after the condensation process. This is because the inlet temperature of the fresh air at state 1 is normally higher than that of the dry air outlet at state 4. In this cycle, the air volumetric flow rate can be adjusted based on the required air temperature and the amount of the useful heating capacity, while the dehumidifying process from state 3 (or 3′) to 4 is necessary for the continuous operation of the heat pump system.

3. Mathematical model

This section focuses on a numerical model developed to analyse moisture removal, dry air heating, and moisture absorption in air cycles. The heat transfer interactions between the working fluids (CO_2 and air) within fin-and-tube heat exchangers were investigated separately during the evaporation and condensation processes [27]. Details of the air–fan model can be found in [28]. The following assumptions were adopted in this study:

The compressor operates adiabatically but not isentropically.
Heat losses within the heat pump and air cycle are negligible.
Pressure drops during heat exchange are negligible.
Airflow within the ducts is maintained with negligible pressure drops and no leakage.
The moisture absorption process is considered isenthalpic.
The expansion valve is assumed to operate under isenthalpic conditions.

3.1. Compressor model

The mass flow rate of a single semi-hermetic reciprocating compressor ($\dot{m}_{comp}$) can be defined as:

$$\dot{m}_{comp} = \eta_v \times V_{s\_ref} \times \rho_{suc} \times f/f_{ref} \quad (1)$$

where ρ_{suc} is the density of the refrigerant at the suction state, f is the motor speed frequency, V_{s_ref} is a reference displacement rate at a certain frequency f_{ref}, and η_v is the volumetric efficiency for the Bitzer

compressor 4HTE-20K [29], which can be determined from:

$$\eta_v(r,f) = 1.071 - 0.2708r + 6.83 \times 10^{-3} f + 3.476 \times 10^{-2} r^2 - 2.512 \times 10^{-4} rf - 3.767 \times 10^{-5} f^2 \quad (2)$$

where r is the compression ratio.

The power required for compression work ($\dot{W}_{comp}$) can be calculated from:

$$\dot{W}_{comp} = \frac{\dot{m}_{comp}(h_{dis\_isentr} - h_{suc})}{\eta_{isentr}} \quad (3)$$

where h_{dis_isentr} is a specific enthalpy at the discharge state during an isentropic compression process, h_{suc} is the specific enthalpy at the compressor suction state, and η_{isentr} is the isentropic efficiency, which can be determined from [29]:

$$\eta_{isentr}(r,f) = 0.5199 - 7.183 \times 10^{-2} r + 1.074 \times 10^{-2} f + 1.064 \times 10^{-2} r^2 - 3.612 \times 10^{-4} rf - 7.694 \times 10^{-5} f^2 \quad (4)$$

3.2. States and energy conversion of the air

Dew point temperature of air (T_{dew}) can be calculated based on the correlation established by Alduchov and Eskridge in 1996 [30], namely:

$$T_{dew} = B_1 \left[\ln\left(\frac{RH}{100}\right) + \frac{A_1 \times T}{B_1 + T} \right] / \left[A_1 - \ln\left(\frac{RH}{100}\right) - \frac{A_1 \times T}{B_1 + T} \right] \quad (5)$$

where RH is the relative humidity, T is a real-time temperature of air, and A_1 and B_1 are the constants based on the measurements, in which $A_1 = 17.625$ and $B_1 = 243.04^{\circ}$C.

The pressure of water vapour inside the air (P_w) can be calculated from:

$$P_w = RH \times P_{w\_sat}/100 \quad (6)$$

where P_{w_sat} is the saturated water vapour pressure, which can be described as [30]:

$$P_{w\_sat} = \exp[(T_{w\_cri} + 273.15)/(T + 273.15) \times (a_1 \times \partial + a_2 \times \partial^{1.5} + a_3 \times \partial^3 + a_4 \times \partial^{3.5} + a_5 \times \partial^4 + a_6 \times \partial^{7.5})] \times P_{w\_cri} \quad (7)$$

where T_{w_cri} is the critical temperature of water which equals 373.95 °C, P_{w_cri} is the critical pressure of water, which is 220.64 bar, a_1 to a_6 are the constants found in the reference [31], and ∂ is the temperature ratio, which can be calculated from:

$$\partial = 1 - \frac{T + 273.15}{T_{w\_cri} + 273.15} \quad (8)$$

Enthalpy of the air (h_{air_tot}) can be determined with the consideration of the humidity ratio (x), heat contained in the dry air (h_{air_dry}) and the moisture content (h_w), respectively, namely:

$$h_{air\_tot} = h_{air\_dry} + xh_w \quad (9)$$

where each part can be calculated from:

$$h_{air\_dry} = Cp_{air} \times T \quad (10)$$

$$h_w = Cp_w \times T + h_{w\_sa} \quad (11)$$

$$x = 0.62198 \times P_w/(P_{amb} - P_w) \quad (12)$$

where Cp_{air} is the specific heat of dry air at an atmospheric pressure ($P_{amb} = 1.01325$ bar), of which the average value is around 1.005 kJ/kg·K [32], Cp_w is the specific heat of water vapour which equals to 1.86 kJ/kg·K, h_{w_sa} is the enthalpy of saturated water vapour at 0 °C, which is 2501.3 kJ/kg [33].

Then, the absolute humidity (AH) can be determined from:

$$AH = P_w/[R_w \times (T + 273.15)] \quad (13)$$

where R_w is the specific gas constant of water vapour, where $R_w = 461.495$ J/kg·K [34].

Total heat change ($\Delta\ \dot{Q}_{air\_tot}$) from the real-time air temperature (T) to the outlet temperature of the evaporator (T_{out}) can be determined from:

$$\Delta\dot{Q}_{air\_tot} = \dot{V}_{air}\,\overline{\rho}_{air} \times (h_{in} - h_{out}) \quad (14)$$

where $\dot{V}_{air}$ is the volumetric flow rate of air, $\overline{\rho}_{air}$ is the average density of air, and h_{in} and h_{out} are the enthalpies at the inlet and outlet of the evaporator, respectively.

The change of the latent heat ($\Delta\dot{Q}_{air\_lat}$) is due to the moisture coming out of the air. The process occurs from the dew point temperature (T_{dew}) down to the outlet temperature of the evaporator (T_{out}), hence, the variation of the latent heat can be described as:

$$\Delta\dot{Q}_{air\_lat} = \dot{V}_{air}\overline{\rho}_{air} \times (h_{in} - h|_{T=T_{in}, x=x_{out}}) \quad (15)$$

where x_{out} is the humidity ratio at the outlet of the evaporator.

The change of the sensible heat ($\Delta\dot{Q}_{air\_sen}$) can be determined based on the temperature difference at the inlet and outlet, respectively, which is:

$$\Delta\dot{Q}_{air\_sen} = \dot{V}_{air}\overline{\rho}_{air} \times Cp_{air}(T_{in} - T_{out}) \quad (16)$$

where T_{in} and T_{out} are the temperatures at the inlet and outlet of the evaporator, respectively.

Finally, the amount of the water vapour to be condensed can be worked out from:

$$\dot{m}_{w\_rem} = \dot{V}_{air}\overline{\rho}_{air}(x_{in} - x_{out}) \quad (17)$$

where x_{in} and x_{out} are the humidity ratios of air at the inlet and outlet of the evaporator.

3.3. Evaporator and gas cooler

The Reynolds number based on collar diameter (Re_{Dc}) can be defined as:

$$Re_{Dc} = \frac{\dot{m}_{air} d_c}{u_{air} A_c} \quad (18)$$

where $\dot{m}_{air}$ is air mass flow rate, d_c is fin collar diameter, u_{air} is air dynamic viscosity, and A_c is minimum flow area.

The Air Nusselt number (Nu) defined with the Reynold number (Re_{Dc}) [35], can be determined from [36]:

$$\begin{cases} Nu = 0.3 + \left(\dfrac{0.62 {Re_{Dc}}^{0.5} {Pr_{air}}^{\frac{1}{3}}}{1 + \left(\frac{0.4}{Pr_{air}}\right)^{\frac{2}{3}}}\right)^{\frac{1}{4}} Re_{Dc} < 1000 \\ Nu = j Re_{Dc} {Pr_{air}}^{\frac{1}{3}} 1000 \le Re_{Dc} \le 20000 \\ Nu = 0.35 {Re_{Dc}}^{0.6} {Pr_{air}}^{0.36} \left(\dfrac{P_t}{P_l}\right)^{0.2} Re_{Dc} > 20000 \end{cases} \quad (19)$$

where j is a Colburn j-factor, which can be derived from:

$$j = 0.086 {Re_{Dc}}^{P_3} M^{P_4} \left(\frac{Fp}{d_c}\right)^{P_5} \left(\frac{Fp}{D_h}\right)^{P_6} \left(\frac{Fp}{P_t}\right)^{-0.93} \quad (20)$$

where

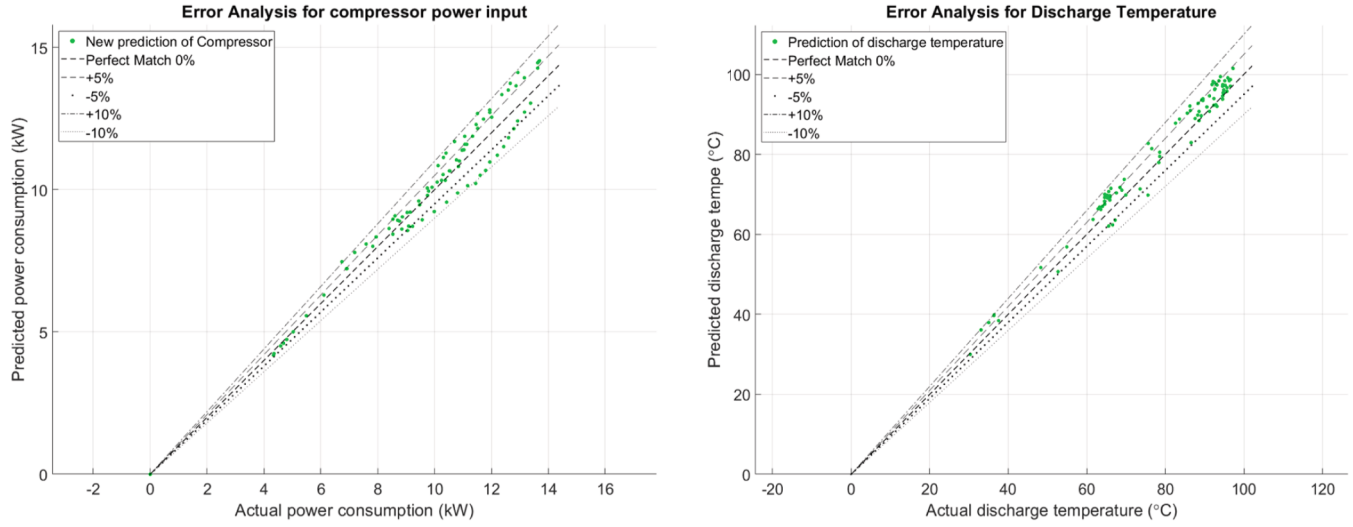

(a) Compressor power (b) Discharge temperature

Fig. 4. Error analysis of the numerical model for the 4HTE-20 K compressor.

$$P_3 = -0.361 - 0.042 M log Re_{Dc} + 0.158 log M^* \left(\frac{Fp}{d_c}\right)^{0.41} \tag{21}$$

$$P_4 = -1.224 - \frac{0.076\left(\frac{P_l}{D_h}\right)^{1.42}}{log Re_{Dc}} \tag{22}$$

$$P_5 = -0.083 - \frac{0.058M}{log Re_{Dc}} \tag{23}$$

$$P_6 = -5.735 + 1.21 log Re_{Dc} \tag{24}$$

where M is number of tube rows, Fp is fin pitch, D_h is hydraulic diameter, Pr_{air} is air Prandtl number, P_t is transverse tube pitch, and P_l is longitudinal tube pitch.

The Air-side heat transfer coefficient (h_o) can be defined as:

$$h_o = \frac{Nu^* k_{air}}{d_c} \tag{25}$$

where k_{air} is air thermal conductivity.

The CO_2 Reynolds number (Re_{CO_2}) can be defined as:

$$Re_{CO_2} = \frac{\dot{m}_{CO_2} d_i}{u_{CO_2} A_i} \tag{26}$$

where $\dot{m}_{CO_2}$ is CO_2 mass flow rate,d_i is tube inner diameter, u_{CO_2} is CO_2 dynamic viscosity, and A_i is CO_2 flow area.

The CO_2 Nusselt number (Nu_{CO_2}) can be calculated as:

$$\begin{cases} Nu_{CO_2} = \dfrac{\frac{f}{8}(Re_{CO_2} - 1000) Pr_{CO_2}}{1 + 12.7\sqrt{\frac{f}{8}}\left(Pr_{CO_2}^{\frac{2}{3}} - 1\right)} & Re_{CO_2} > 3000 \\ Nu_{CO_2} = 3.66 Re_{CO_2} & \leq 3000 \end{cases} \tag{27}$$

where Pr_{CO_2} is CO_2 Prandtl number and f is friction factor, that is:

$$f = (0.79 log(Re_{CO_2}) - 1.64)^{-2} \tag{28}$$

$$Pr_{CO_2} = \frac{Cp_{CO_2} u_{CO_2}}{k_{CO_2}} \tag{29}$$

where Cp_{CO_2} is CO_2 specific heat and k_{CO_2} is the CO_2 thermal conductivity.

The CO_2-side heat transfer coefficient (h_i) can be defined as:

$$h_i = \frac{Nu_{CO_2}{}^* k_{CO_2}}{d_i} \tag{30}$$

where d_i is tube inner diameter.

The fin parameter (m) can be defined as:

$$m = \sqrt{\frac{2h_o}{k_{fin}\Delta_f}} \tag{31}$$

where k_{fin} is fin thermal conductivity and Δ_f is fin thickness.

The fin efficiency (η_{fin}) can be defined as:

$$\eta_{fin} = \frac{tanh(mL_e)}{mL_e} \tag{32}$$

where L_e is effective fin length.

The overall heat transfer coefficient (UA) can be defined as:

$$UA = \left(\frac{1}{\eta_{fin} h_o A_o} + \frac{\Delta x}{k_{wall} A_m} + \frac{1}{h_i A_i}\right)^{-1} \tag{33}$$

where A_o is outer surface area, k_{wall} is wall thermal conductivity, A_m is mean conduction area, A_i is CO_2 flow area, and Δx is tube wall thickness.

The heat transfer rate (Q) can be defined as:

$$\dot{Q} = UA(T_{air} - T_{CO_2}) \tag{34}$$

where T_{air} is CO_2 temperature, T_{CO_2} is CO_2 temperature, and UA is mean conduction area.

3.4. Moisture absorption and system performance

The moisture absorption rate ($\dot{m}_{w\_abs}$) from the wet material can be calculated from:

$$\dot{m}_{w\_abs} = \dot{V}_{air} \bar{\rho}_{air} (x_{abs} - x_{con\_air}) \tag{35}$$

where x_{con_air} is the humidity ratio after the dry-air heating process through the condenser and x_{abs} is the humidity ratio after absorbing the moisture from the wet material, of which the maximum humidity ratio

can be described as:

$$x_{abs\_max} = x_{abs}|_{RH=RH_{max},h=h_{con\_air\_out}} \tag{36}$$

where $h_{con\_air\_out}$ is the air enthalpy at the outlet of the condenser and RH_{max} is the relative humidity of air after the moisture absorption process.

If the mass of moisture containing in the material is defined as $m_{material\_w}$, hence, the time required for drying up the material can be determined from:

$$t_{material\_w} = \frac{m_{material\_w}}{\dot{m}_{w\_abs}} \tag{37}$$

The term of SMER is employed to describe the ratio of the amount of the water removed from a material to the total energy consumed for compressor (W_{comp}) and fan (W_{fan}) [37]:

$$SMER = \frac{m_{material\_w}}{W_{comp} + W_{Fan}} \tag{38}$$

For the heat pump system, regardless of whether air runs in an open or closed-looped cycle, both the heating and cooling processes of the heat pump are involved in the drying process, i.e. the heating part is used to heat the dry air to a higher temperature so that it can absorb more moisture, while the cooling part is used to cool down the wet air, and concurrently, to remove the moisture from the air. Therefore, the combined COP for the heat pump dryer can be determined from:

$$COP_{hp} = \frac{\dot{Q}_{cool} + \dot{Q}_{heat}}{\dot{W}_{comp} + \dot{W}_{fan}} \tag{39}$$

where $\dot{Q}_{cool}$ and $\dot{Q}_{heat}$ are the useful cooling and heating capacities generated by the heat pump, respectively, and $\dot{W}_{comp}$ and $\dot{W}_{fan}$ are the power input for the compressor and air-cooled fan, respectively.

4. Validation

The numerical model for the compressor type 4HTE-20K has been validated against the published experimental data with acceptable agreements, i.e.: within ± 10 % [38], and this speed-driven compressor model has significantly improved the model accuracy at the low-speed frequencies (i.e. lower than 40 Hz), compared to the existing model [39]. Fig. 4 illustrates the error analysis between the simulation results and experimental results for compressor power inputs and discharge temperatures, respectively. The predicted values demonstrate an alignment with the experimental measurements across the full operating range, which indicates that the model captures both thermodynamic and performance characteristics effectively. Most of the validation points fall within the ± 5 % error, while only a small number approach the ±10 % range, typically under high-load conditions where measurement uncertainty is bigger.

The fin-and-tube heat exchangers with the geometric configuration listed in Table 2 and Table 3 for the gas cooler and evaporator have been validated from the previous study [40], thus those values have been adopted in the case study in Section 5.

5. Case study

Since the mathematical model of CO_2 compressor, i.e.: Bitzer 4HTE-20K has been fully developed and validated, it will be selected for use in this case study. Table 1 includes some initial conditions set for this numerical model. The geometries and dimensions of the fin-and-tube heat exchangers have been included in the existing study for evaporator [40] and gas cooler [41], as shown in Table 2 and Table 3, respectively. The study aims to compare the thermodynamic behaviour of open-loop and closed-loop cycles under identical conditions, rather than perform a full climatic sensitivity analysis. The simulation was conducted under characteristic operating conditions with ambient air at 40 °C and relative humidity of 50 %, which represent typical hot and humid climates where heat pump drying systems are commonly used. The chosen 40 °C air inlet temperature ensures effective heat exchange in all three air cycles and provides consistent conditions for fair performance comparison; otherwise, in the open-loop air cycle with a wet air outlet, the temperature difference between the inlet air and the evaporator would be insufficient. The air mass flow rate (0.5–1.0 kg/s) reflects the operational range of medium-scale industrial dryers. Cotton was used as the drying material due to its well-established moisture transport behaviour and suitability for performance benchmarking.

Table 1
Initial conditions for the model.

Type of the air cycle	Open and closed-looped
Drying material	Cotton
Maximum withstand temperature, $T_{material\_max}$	90 °C
Mass of the moisture contained, $m_{material\_w}$	5 kg
Discharge pressure of CO_2 heat pump, P_{dis}	80 bar
Gas cooler temperature, T_{gas}	45 °C
Relative humidity of ambient air, RH_{amb}	50 %
Ambient temperature, T_{amb}	40 °C
Evaporation temperature, T_{ev}	5 °C
Suction superheat, ΔT_{super}	$[10K, 20K]$
Minimum pinch point temperature difference	5 °C
Relative humidity of air after moisture absorption, RH_{max}	80 %

Table 2
Geometry parameters for the evaporator.

Fin thickness, d_f	0.15 mm
Tube inner diameter, d_i	8.2 mm
Tube outer diameter, d_o	9.52 mm
Fin pitch, F_p	1.2 mm
Tube length, L	420 mm
Number of tube rows, M	4
Transverse pitch, P_t	25.4 mm
Longitudinal pitch, P_l	22 mm

5.1. Air-heating process

The simulation results for the air-heating processes occurred in the CO_2 gas cooler have been demonstrated in the following three scenarios. For clarity, "Segment Number" in the figures refers to the spatial indexing of the evaporator and gas cooler along the flow direction, where heat and mass transfer interactions between CO_2 and air are calculated. The "CO_2 temperature" shown in the figures represents the refrigerant temperature profile inside the corresponding heat exchanger (either the gas cooler or evaporator) along the same segmented flow path.

For the closed-loop air cycle, as shown in Fig. 5(a), there is only one mass flow rate that can make the cycle match in both air inlet and outlet conditions of the gas cooler, before being utilised for absorbing the moisture from the wet material. The heating capacity generated in the closed-loop air cycle is 15.7 kW when the mass flow rate is set as 0.69 kg/s. For the open-loop air cycle with the wet air outlet, as shown in Fig. 5(b), the inlet air temperatures are different due to various air mass

Table 3
Geometry parameters for the gas cooler.

Fin thickness, d_f	0.15 mm
Tube inner diameter, d_i	6.35 mm
Tube outer diameter, d_o	7.37 mm
Fin pitch, F_p	1.2 mm
Tube length, L	225 mm
Number of tube rows, M	4
Transverse pitch, P_t	25.4 mm
Longitudinal pitch, P_l	22 mm

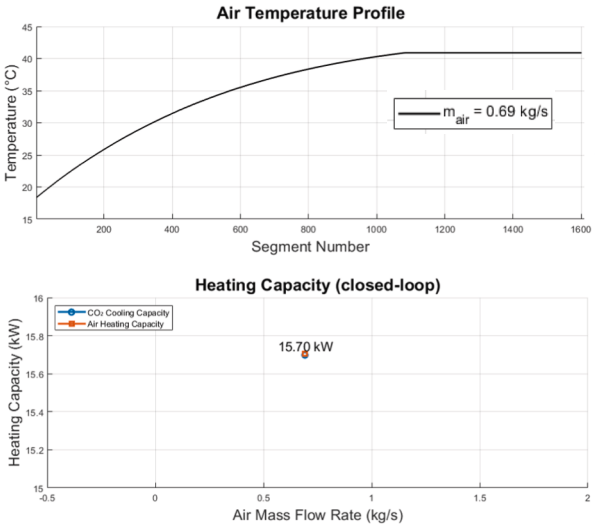

(a) Closed-loop air cycle

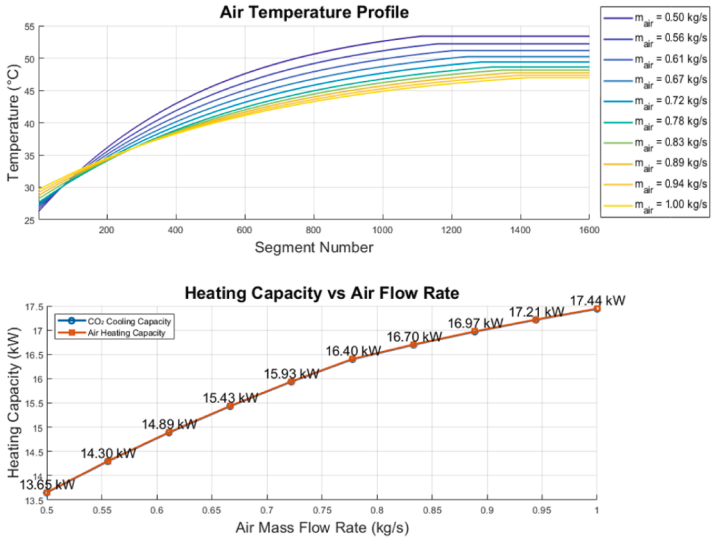

(b) Open-loop air cycle with wet air outlet

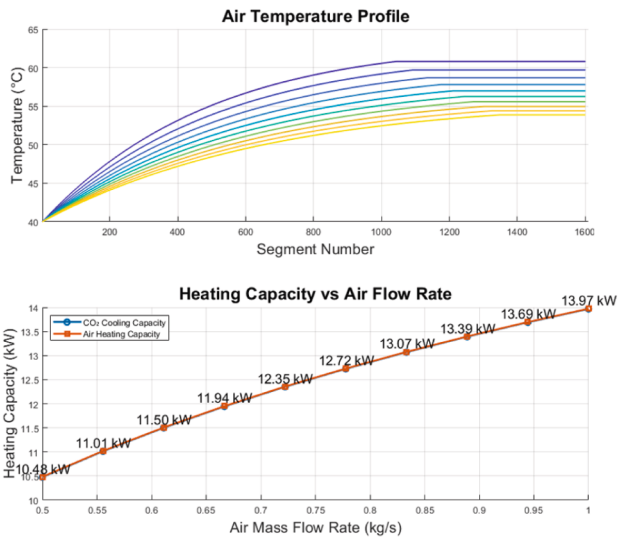

(c) Open-loop air cycle with dry air outlet

Fig. 5. Air heating process in the CO_2 gas cooler.

flow rates and the fresh air entering the cycle initiating from the evaporator. Therefore, the inlet air temperatures change from 26.26 °C to 29.65 °C as the mass flow rates increases from 0.5 kg/s to 1 kg/s; concurrently, the heating capacity increase from 13.65 kW to 17.44 kW. The air temperature exiting from the gas cooler increases from 47.12 °C to 54. 58 °C when the air mass flow rates decrease from 1 kg/s to 0.5 kg/s. When it is an open-loop air cycle with the dry air outlet, as shown in Fig. 5(c), the air inlet temperature remains at 40 °C while the air outlet temperatures decrease with the air mass flow rates, i.e.: from 53.87 °C to 60. 80 °C with the mass flow rate decreasing from 1 kg/s to 0.5 kg/s. Accordingly, the heating capacity generated during the process ranges between 10.48 kW and 13.97 kW.

5.2. Moisture-absorption and dehumidification process

Since the fresh or dry air has been heated up to a higher temperature through the CO_2 gas cooler, the air will then absorb the moisture by passing through the wet material, followed by the dehumidification process occurring in the evaporator. For the closed-loop air cycle, as shown in Fig. 6, when the air mass flow rate is 0.69 kg/s, the air temperature entering the evaporator is 24.43 °C after losing some heat due to the moisture absorption. During the evaporation process, the air temperature firstly decreases more obviously down to 20.83 °C, followed by a slower decline to 18.94 °C. The temperature decrease is firstly due to the sensible heat change, followed by both sensible and latent heat change with the moisture coming out. As indicated in Fig. 6 (c), the humidity ratio remains constant at 15.5 g/kg $_{dry\ air}$ during the initial stage, and then decreases to 13.74 g/kg $_{dry\ air}$. The cooling capacity generated during the evaporation process is 6.58 kW, as shown in Fig. 6(d).

For the open-loop air cycle with wet air outlet, as shown in Fig. 7, the fresh air will pass through the evaporator to get rid of the self-contained moisture first. With the air mass flow rates ranging from 0.5 kg/s to 1 kg/s, as shown in Figs. 7(a) and (b), CO_2 temperatures increase from 5 °C to around 25 °C at the air mass flow rate of 1 kg/s (and reaches around 22.63 °C at a mass flow rate of 0.5 kg/s), while the air temperatures decrease from 40 °C to 28 °C at the mass flow rate of 0.5 kg/s. It is noted that the cooling process also involves the dehumidification in the

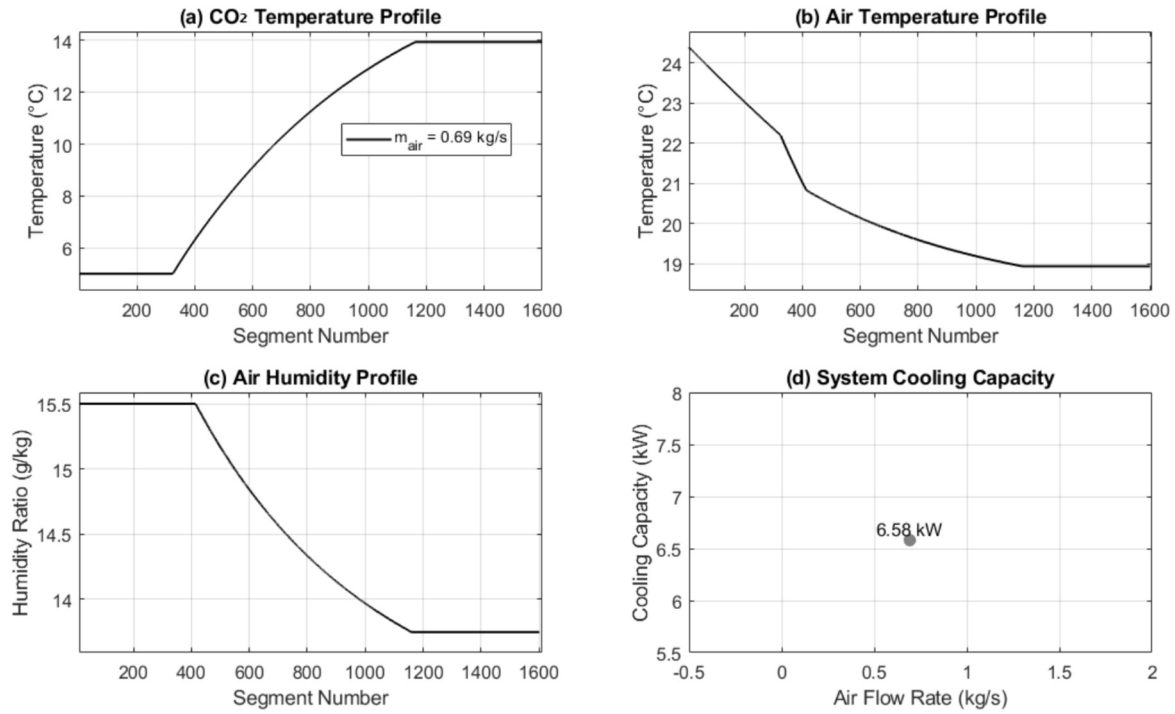

Fig. 6. Moisture-absorption and dehumidification process for a closed-loop air cycle.

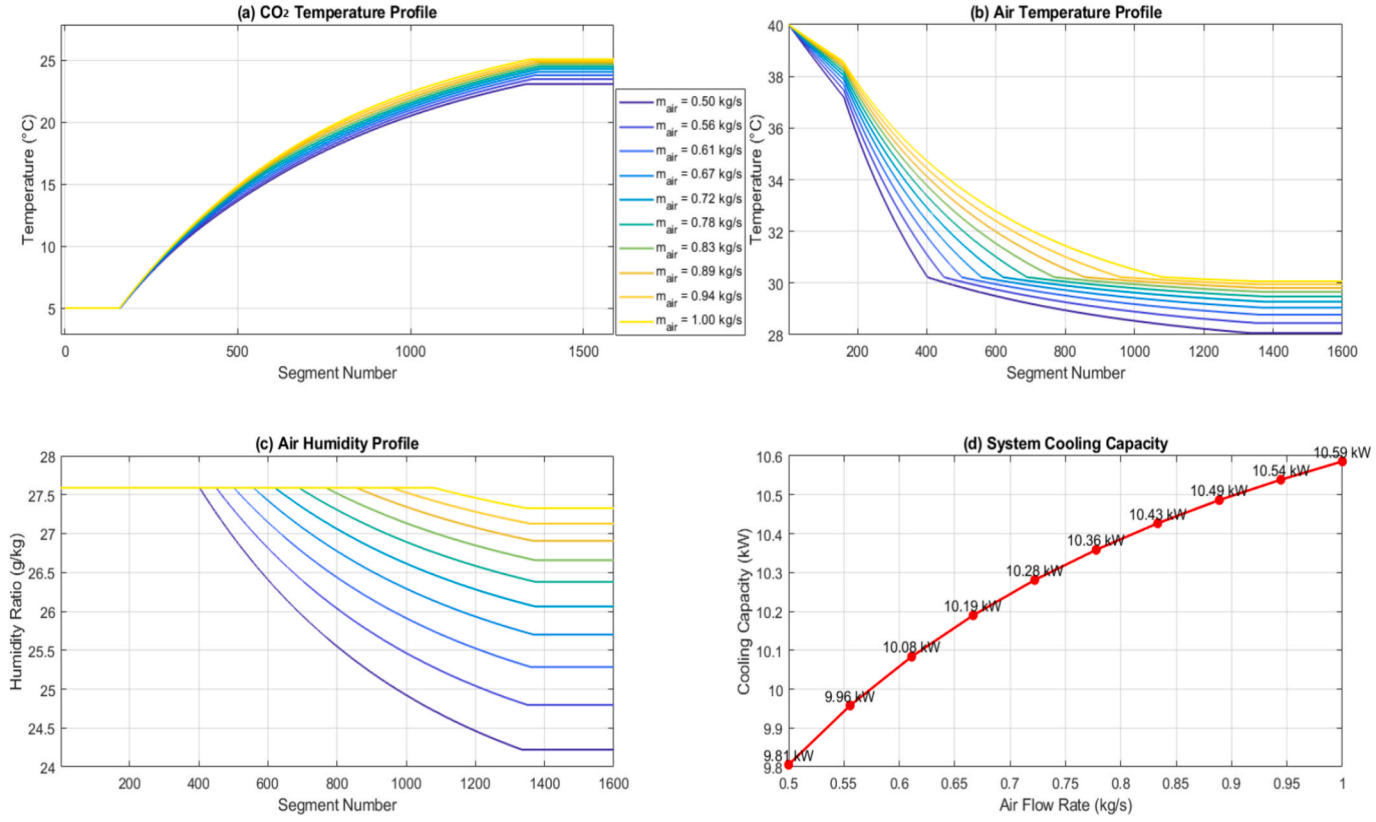

Fig. 7. Moisture-absorption and dehumidification process for an open-loop air cycle with wet air outlet.

later stage of the evaporation, which is indicated by the humidity ratio in Fig. 7(c). Lower mass flow rate leads to more moisture being released from the evaporator, i.e.: the humidity ratio decreases from 27.6 g/kg $_{dry\ air}$ to 24.25 g/kg $_{dry\ air}$ at the mass flow rate of 0.5 kg/s. In addition, the cooling capacity generated increases from 9.81 kW to 10.59 kW with the air mass flow rate increasing from 0.5 kg/s to 1 kg/s.

For the open-loop air cycle with a dry air outlet, as shown in Fig. 8, since the fresh air enters the CO_2 gas cooler at different mass flow rates, various air temperatures are achieved at the outlet of the gas cooler. Following the moisture absorption process, the humidity ratio varies due

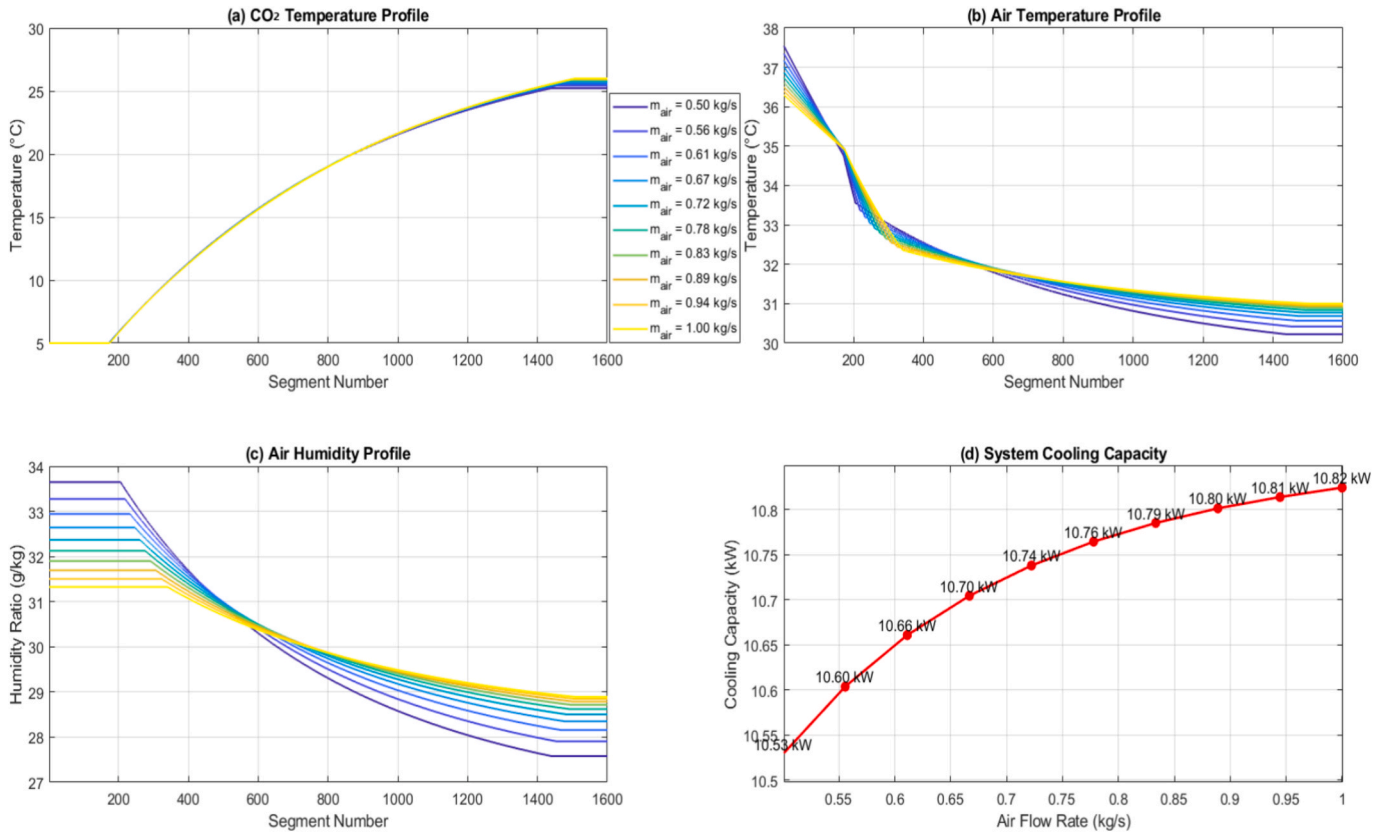

Fig. 8. Moisture-absorption and dehumidification process for an open-loop air cycle with dry air outlet.

to differences in absorption capacity at different air temperatures, as shown in Figs. 8(b) and (c). When the air mass flow rate is 1 kg/s, the air temperature decreases from 36.32 °C to 31.05 °C, with the humidity ratio decreasing from 31.32 g/kg $_{\text{dry air}}$ to 28.92 g/kg $_{\text{dry air}}$. At meanwhile, the CO_2 temperature increases from 5 °C to around 25 °C inside evaporator. The cooling capacity increases with the air mass flow rate, i.e.: from 10.53 kW to 10.82 kW within the operating ranges of the air mass flow rates between 0.5 kg/s and 1 kg/s.

In comparison among three air cycles, it can be found that the open-loop air cycle with dry air outlet can generate a larger cooling capacity under the same air mass flow rate, compared to that with wet air outlet and the closed-loop air cycle. This is mainly because that the moisture was absorbed from the wet material before being dehumidified in the air cycle with dry air outlet, and the air temperature after being heated in the CO_2 gas coolers is relatively high compared to that of the closed-loop air cycle.

5.3. *Drying performance*

The drying performance under three different air cycles have been described in Figs. 9 to 11. For the closed-loop air cycle and the open-loop air cycle with dry air outlet, it is quite direct that the moisture absorbed from the wet material will be dehumidified during the subsequent evaporation process. However, for the open-loop air cycle with wet air outlet, since the fresh air without moisture absorption will enter the evaporator first, the dehumidification process will remove the self-contained moisture from the fresh air, indirectly enabling it capable of absorbing more moisture from the wet material.

Fig. 9 indicates the drying performance in the closed-loop air cycle, with the drying time of 68.49 min, SMER of 0.3501 kg/kWh, and the COP of 1.73 when the air mass flow rate is fixed as 0.69 kg/s. For the open-loop air cycle with wet air outlet, as shown in Fig. 10, the material drying time increases from 49.50 min to 319.37 min with the air mass flow rate ranging from 0.5 kg/s to 1 kg/s. The SMER decreases from 0.4846 kg/kWh to 0.0767 kg/kWh. The variation of the humidity ratio at the inlet and outlet of the evaporator decreases with the increase of the air mass flow rates (as described in Fig. 7(c)), in other words, the reduced residence time inside the evaporator lowers the extent of water vapour transfer. The COP in this cycle is between 1.89 and 2.31 with the increase of air mass flow rates. It needs to be clarified that the sharp increase in drying time near an air mass flow rate of 1.0 kg/s is primarily caused by the combined effects of reduced air residence time, weakened heat transfer, and diminished moisture-removal potential. At very high flow rates, the air passes through the gas cooler too quickly to absorb sufficient heat, which leads to a lower outlet air temperature and a reduced ability to carry moisture away from the material. This also decreases the refrigerant temperature lift, weakening both the heating and dehumidification capacities of the system.

Fig. 11 describes the drying performance in the open-loop air cycle with dry air outlet. The drying time increases from 27.77 min to 34. 68 min with the air mass flow rate, while the SMER decreases from 0.8640 kg/kWh to 0.7060 kg/kWh. The COP in this cycle under the same mass flow rate is slightly lower than that of the cycle with wet air outlet. This mainly results from the reduced heating capacity of the air, caused by its higher inlet temperature and the pinch point temperature difference of 5 °C, which limits the final heating temperature. In contrast, when the outlet air is wet, the lower inlet temperature allows for a more noticeable temperature rise.

Although the initial moisture content of the drying material was not directly varied in this study, its influence on system performance can be effectively interpreted. A higher initial moisture content generally increases the latent heat load on the evaporator, which results in greater energy demand and a longer drying period. Consequently, the SMER may decrease due to higher energy consumption per unit of water removed. Similarly, the COP can be affected, as more compressor work is required to maintain the desired temperature lift under higher

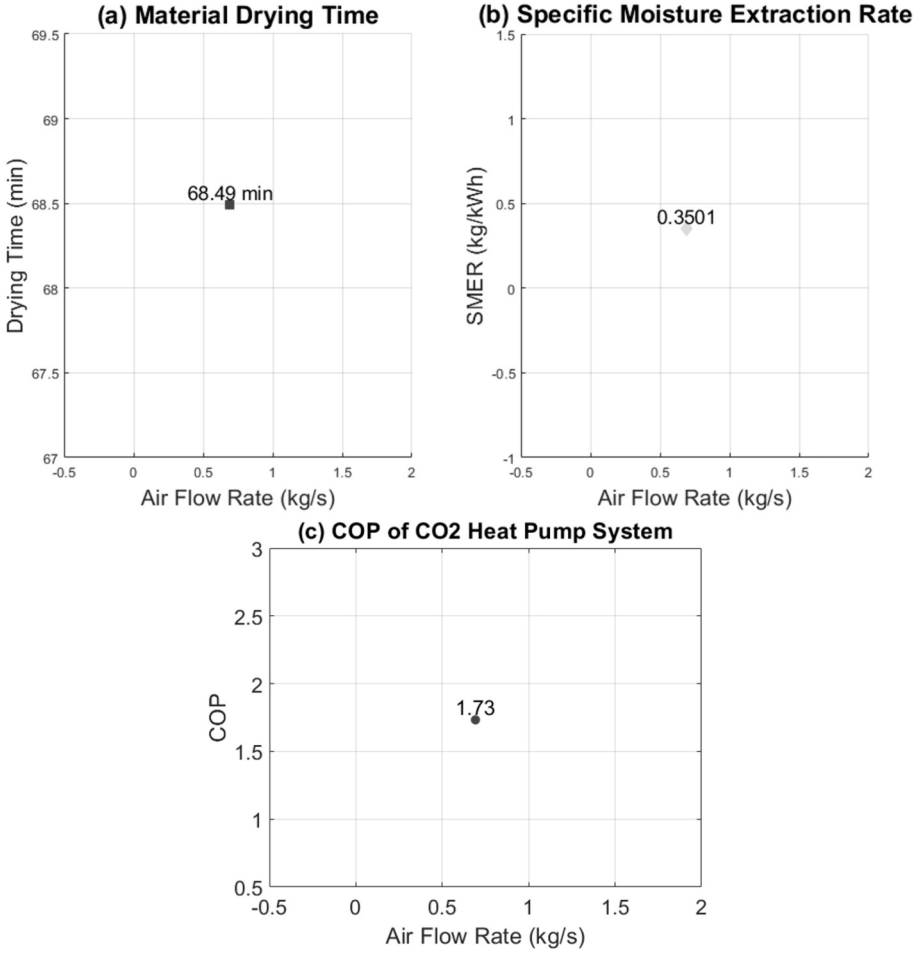

Fig. 9. Drying performance of the closed-loop air-cycle.

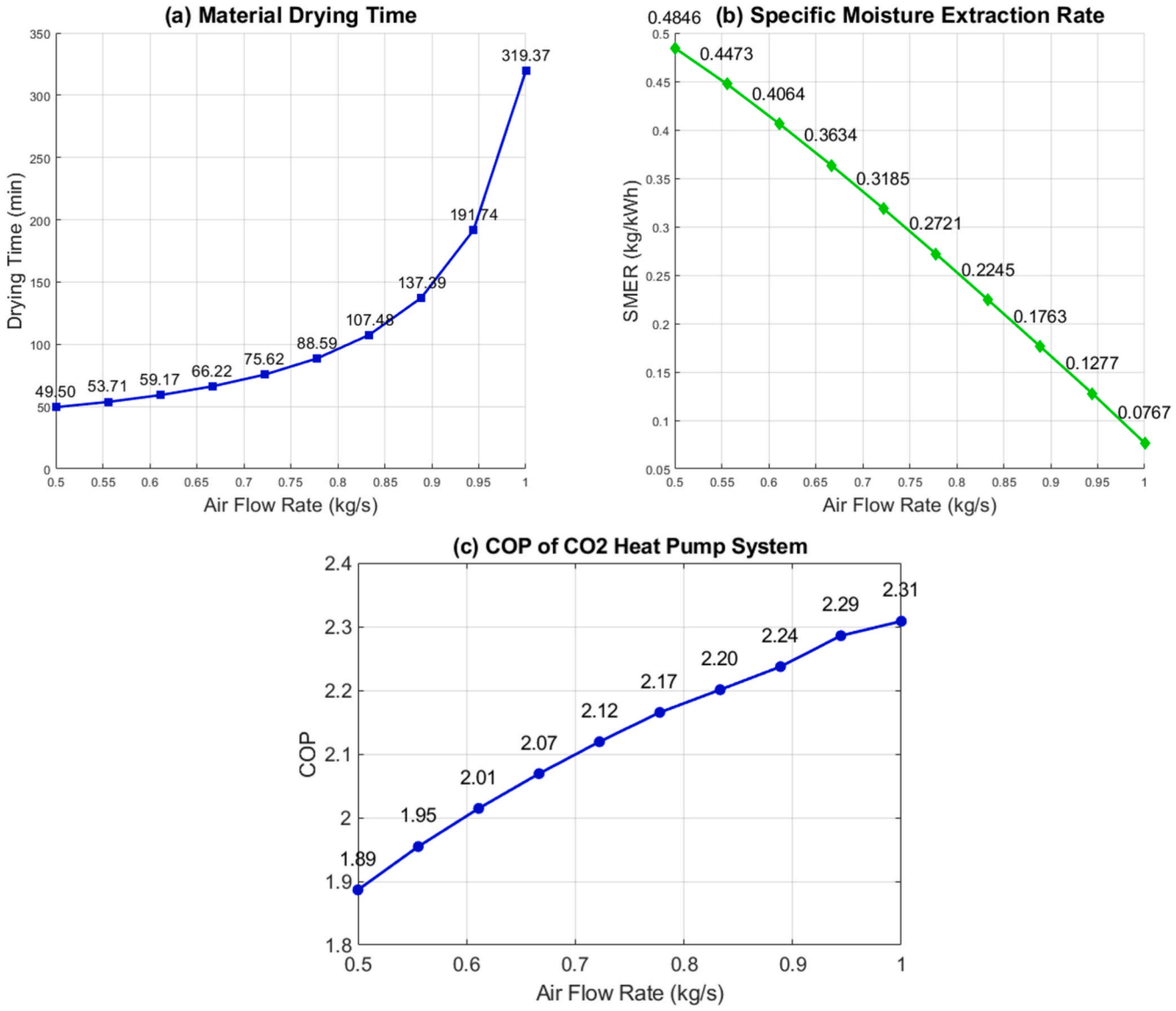

Fig. 10. Drying performance of the open-loop air cycle with wet air outlet.

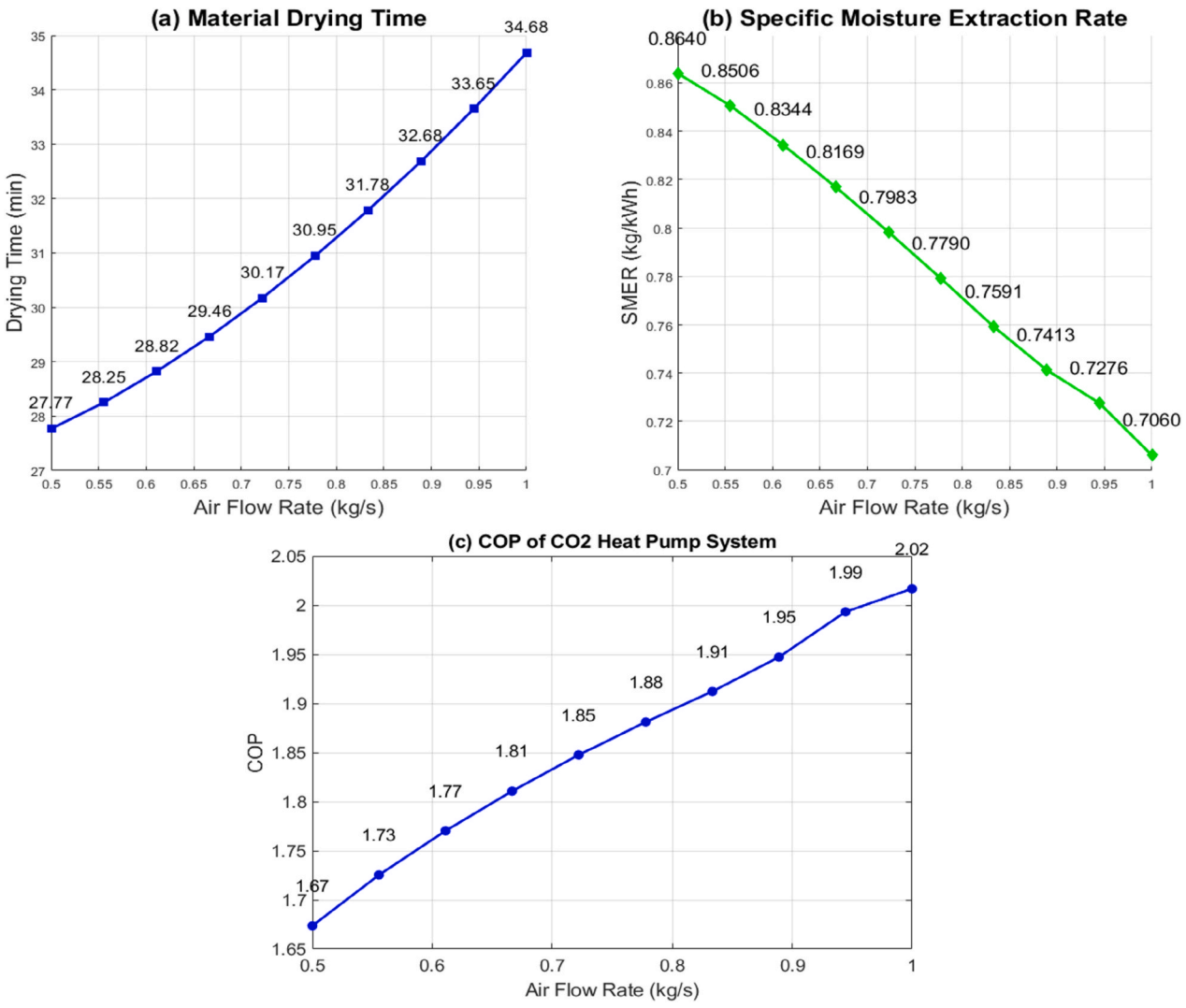

Fig. 11. Drying performance of the open-loop air cycle with dry air outlet.

moisture loads. In contrast, materials with lower initial moisture content allow quicker moisture removal and reduced compressor duty, which improves both SMER and COP. These trends align with the thermodynamic behaviour of the open-loop and closed-loop air cycles analysed in this study.

In real applications, CO_2 heat pump dryers face several practical challenges. Because the system operates at very high pressures (often above 75 bar in a transcritical cycle), the design and installation must ensure safety and reliability. This requires strong materials, secure sealing, and regular maintenance to prevent leaks or failures. Operating such systems also requires appropriate safety controls and skilled personnel. Although these practical issues were not the main focus of this study, they are important for real-world use.

The findings of this study offer useful guidance for practical dryer design. The open-loop air cycle with a dry air outlet provides the balance between energy efficiency and drying performance, which makes it a promising choice for industrial applications where product quality and energy use are critical. The simulation results suggest that optimizing air flow rate and outlet air conditions can help manufacturers achieve shorter drying time and higher system efficiency while maintaining safe and stable operation.

6. Conclusions and future work

The comparative conceptual analysis for the CO_2 heat pump system integrated with open-loop and closed-loop air cycles have been conducted. Several conclusions can be drawn from this study:

1. The configuration of the CO_2 heat pump system for the drying purposes has been proposed. The physical models for both open-loop and closed-loop air cycles have been developed, and their working principles illustrated using psychrometric charts. Unlike the conventional closed-loop air cycle that relies on air recirculation, the open-loop air cycle operates solely with fresh ambient air, which offers a fundamentally different air-handling strategy.
2. The mathematical model for the selected compressor has been developed and validated with acceptable agreement. The influence of moisture variation has been incorporated into the fin-and-tube heat exchanger design, which functions as both the gas cooler and the evaporator. The comparative performance of the three cycles, which are assessed through SMER, COP, and drying time, demonstrates the effect of air-cycle configuration on overall system behaviour.
3. In the case study conducted at an ambient temperature of 40 °C, the simulation compares the three cycles over an air mass flow rate ranging from 0.5 kg/s to 1 kg/s. The open-loop air cycle with a wet

air outlet achieves the highest heating capacity, (17.44 kW at the air mass flow rate of 1 kg/s), due to its configuration in which the air is cooled in the evaporator first, enabling a larger temperature rise in the gas cooler. In contrast, the open-loop air cycle with a dry air outlet delivers the highest air outlet temperature after the gas cooler (60.8 °C at the mass flow rate of 0.5 kg/s), which is advantageous for drying as it increases the air's moisture absorption capability.

4. The open-loop air cycle with a dry air outlet operates with a shorter drying time (27.77 min vs. 68.49 min) and with higher drying efficiency (SMER of 0.864 kg/kWh Vs. 0.350 kg/kWh) compared with the closed-loop baseline. The open-loop wet outlet cycle achieves the highest COP of 2.31, that is a 33.5 % increase over the closed-loop COP of 1.73. However, the wet outlet cycle's performance is inconsistent. At a high air flow rate of 1 kg/s, its SMER drops sharply to 0.0767 kg/kWh.
5. Through comparison, the open-loop cycle with a dry air outlet is the superior configuration for drying. It delivers the shortest drying time and the highest SMER, which are the two most critical performance metrics for any dryer. Although the open-loop air cycle with a wet air outlet can achieve a higher COP, this advantage is diminished by its reduced performance at higher flow rates and its significantly poorer drying metrics.

The current model assumes uniform air distribution and steady-state boundary conditions. While these assumptions allow clear thermodynamic comparison, practical implementation may require adjustments for specific materials and drying environments. Future work will include experimental validation, system optimization under varying ambient conditions, and integration with industrial-scale drying processes to improve applicability and reliability. In addition, a comprehensive techno-economic analysis will be conducted to evaluate the commercial viability and optimal configurations of CO_2 heat pump drying systems using both open-loop and closed-loop air cycles.

Declaration of competing interest

The author declare that they have no known competing financial interests or personal relationships that could have appeared to influence the work reported in this paper.

Data availability

Data will be made available on request.

References

[1] Wang J, et al. A comprehensive review and analysis on CO2 heat pump water heaters. Energy Convers Manage: X 2022:100277.
[2] Minea V. Improvements of high-temperature drying heat pumps. Int J Refrig 2010;33(1):180–95.
[3] Jouhara H, et al. High-temperature heat pumps: fundamentals, modelling approaches and applications. Energy 2024;303:131882.
[4] Uthpala T, Navaratne S, Thibbotuwawa A. Review on low-temperature heat pump drying applications in food industry: cooling with dehumidification drying method. J Food Process Eng 2020;43(10):e13502.
[5] Claussen I, Ustad T, Str⍉ Mmen I, Walde P. Atmospheric freeze drying—a review. Drying Technol 2007;25(6):947–57.
[6] Colak N, Hepbasli A. A review of heat pump drying: part 1 – systems, models and studies. Energ Conver Manage 2009;50(9):2180–6.
[7] Ogura H, et al. A control strategy for a chemical heat pump dryer. Drying Technol 2005;23(6):1189–203.
[8] Mujumdar AS. Handbook of industrial drying. CRC press, 2006.
[9] Ho J, et al. An optimisation framework for drying of heat-sensitive products. Appl Therm Eng 2001;21(17):1779–98.
[10] Lawton J. Drying: the role of heat pumps and electromagnetic fields. Phys Technol 1978;9(5):214.
[11] Strommen I, et al. Low temperature drying with heat pumps new generations of high quality dried products. Proceeding in 13th International Drying Symposium (IDS2002). 2002.
[12] Zhou H, Wu W, Zeng T, Hou Y. Experimental study on CO_2 closed-cycle heat pump drying for lemon assisted by ultrasonic pretreatment. J Clean Prod 2025;501:145321.
[13] Xie Y, et al. Coupled investigation of dynamic moist air dehumidification and heat pump drying in a close-cycle dishwasher. Appl Therm Eng 2025;261:125153.
[14] Wu Z, Li Y, Zhou W, Fu Q. Multi-objective optimization of heat pump drying process using NSGA-II and response surface methodology: a case study of sludge. Case Stud Therm Eng 2025;72:106257.
[15] Ni H, Hu P, Li Y. Analysis and optimization of the performance of closed heat pump dryer based on zeotropic mixtures. Appl Therm Eng 2025;260:124916.
[16] Lakshmi Kanthan Bharathi A, Kalaiselvam S. Performance evaluation of low-temperature operated desiccant wheel integrated heat pump drying system for ponyfish (Leiognathus equula) drying. Int J Refrig 2025;173:55–67.
[17] Jo H, et al. Multi-objective optimization of the operation strategies for heat pump tumble dryers with different fabric types. Appl Therm Eng 2025;274:126752.
[18] Hou Y, et al. Effect of intermittent ratio on the performance of a closed-loop heat pump drying system with a novel ternary refrigerant and on the drying characteristics of corn kernels. Int Commun Heat Mass Transfer 2025;161:108541.
[19] Guan X, et al. Research on the performance of heat pump drying system with rock thermal energy storage. Energy 2025;316:134510.
[20] Hou F, et al. Study and optimization of the influence of the water tank temperature on the performance of a solar assisted multi-source heat pump drying system. Appl Therm Eng 2025;259:124922.
[21] Aktekeli B, et al. Experimental study of a novel design bi-fluid based photovoltaic thermal (PVT)-assisted heat pump dryer. Renew Energy 2025;238:121971.
[22] Graban A, Groll E, Braun J, Ziviani D. Review of heat pump tumble clothes dryer energy efficiency and related technologies, 2021.
[23] IRENA, Renewable Solutions in End-Uses, Heat Pump Costs and Markets. International Renewable Energy Agency Abu Dhabi, United Arab Emirates, 2022.
[24] Deymi-Dashtebayaz M, et al. Recent developments in heat pump dryers focusing on methods of supplying and reducing their energy consumption. J Therm Anal Calorim 2024;149(17):9751–75.
[25] Chua KJ, Chou SK, Ho JC, Hawlader MNA. Heat pump drying: recent developments and future trends. Drying Technol 2002;20(8):1579–610.
[26] Mancini F, Minetto S, Fornasieri E. Thermodynamic analysis and experimental investigation of a CO_2 household heat pump dryer. Int J Refrig 2011;34(4):851–8.
[27] Lee B-H, Sian RA, Wang C-C. A rationally based model applicable for heat pump tumble dryer. Drying Technol 2019;37(6):691–706.
[28] Sarkar J, Souvik B, Gopal MR. Transcritical CO_2 heat pump dryer: part 1. Mathematical model and simulation. Drying Technol 2006;24(12):1583–91.
[29] Wang J. Accurate and streamlined approach for modelling hermetic reciprocating compressors, 2025.
[30] Lawrence MG. The relationship between relative humidity and the dewpoint temperature in moist air - a simple conversion and applications. Bull Am Meteorol Soc 2005;86:225–33.
[31] Wagner W, Pruß A. The IAPWS formulation 1995 for the thermodynamic properties of ordinary water substance for general and scientific use. J Phys Chem Ref Data 2002;31(2):387–535.
[32] Weltner K. Measurement of specific heat capacity of air. Am J Phys 1993;61(7):661–2.
[33] Srebric J. Indoor Environmental Control, in Mechanical Engineers' Handbook. p. 1-21.
[34] Mohr PJ, Newell DB, Taylor BN. CODATA recommended values of the fundamental physical constants: 2014. J Phys Chem Ref Data 2016;45(4):043102.
[35] Churchill SW, Bernstein M. A correlating equation for forced convection from gases and liquids to a circular cylinder in crossflow, 1977.
[36] Žukauskas A. Heat transfer from tubes in crossflow. In: Advances in Heat Transfer. Elsevier; 1972. p. 93–160.
[37] Yousaf K, et al. Influence of environmental conditions on drying efficiency and heat pump performance in closed and open loop drying of paddy. Drying Technol 2020;38(16):2217–30.
[38] Wang J, et al. A comprehensive study on a novel transcritical CO_2 heat pump for simultaneous space heating and cooling – concepts and initial performance. Energ Conver Manage 2021;243:114397.
[39] Wang J, et al. An optimisation study on a real-world transcritical CO_2 heat pump system with a flash gas bypass. Energ Conver Manage 2022;251:114995.
[40] Lin K-H, Kuo C-S, Hsieh W-D, Wang C-C. Modeling and simulation of the transcritical CO_2 heat pump system. Int J Refrig 2013;36(8):2048–64.
[41] Sian RA, Wang C-C. Comparative study for CO_2 and R-134a heat pump tumble dryer – a rational approach. Int J Refrig 2019;106:474–91.